27
11-14-79
2-4 to 711 15

UCID- 18314

Lawrence Livermore Laboratory

PHYSICS PARAMETER CALCULATIONS FOR A
TANDEM MIRROR REACTOR WITH THERMAL BARRIERS

B. M. Boghosian, D. A. Lappa, B. G. Logan

November 6, 1979

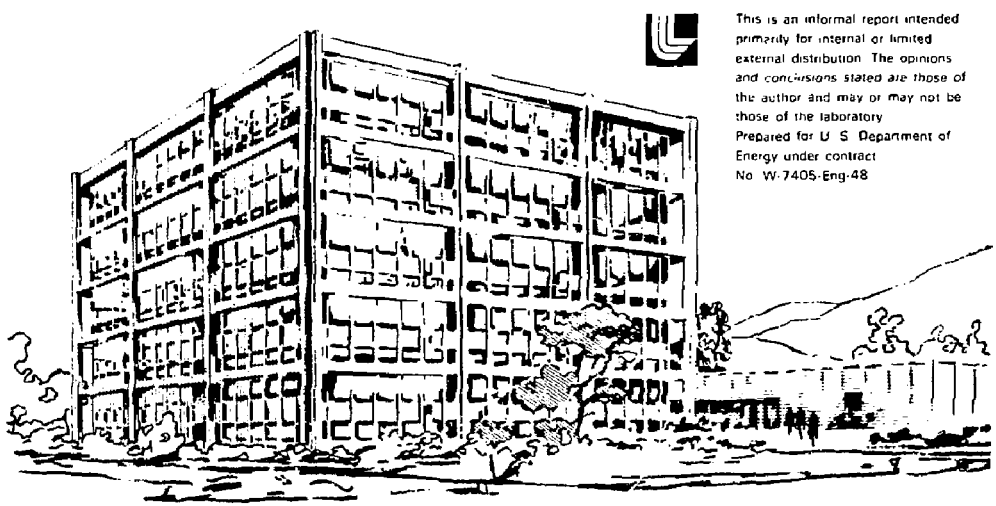

PHYSICS PARAMETER CALCULATIONS FOR A TANDEM MIRROR REACTOR WITH THERMAL BARRIERS

by

B. M. Boghosian, D. A. Lappa, B. G. Logan

Lawrence Livermore Laboratory*

Abstract

We investigate a new idea of enhancing Tandem Mirror Reactor confinement by the addition of thermal barriers. Thermal barriers are localized reductions in potential between the plugs and the central cell, which effectively insulate trapped plug electrons from the central cell electrons. By then applying electron heating in the plug, it is possible to obtain trapped electron temperatures that are much greater than those of the central cell electrons. This, in turn, effects an increase in the plug potential and central cell confinement with a concomitant decrease in plug density and injection power. Ions trapped in the barrier by collisions are removed by the injection of neutral beams directed inside the barrier cell loss cone; these beam neutrals convert trapped barrier ions to neutrals by charge exchange permitting their escape. We describe a zero-dimensional physics model for this type of reactor, and present some preliminary results for Q.

* Performed by LLL for USDOE under Contract W-7405-Eng-48.

I. INTRODUCTION

This paper describes a computer code developed for use by the Fusion Reactor Studies group at the Lawrence Livermore Laboratory to assess the performance of tandem mirror fusion reactors with thermal barriers. A thermal barrier is a potential depression between the plug and the central cell of a tandem mirror that serves to thermally insulate the electrons trapped in the plug and transition region (trapped electrons) from those that are free to traverse the length of the machine (passing electrons). In this way, by applying ECRH in the plug or transition region, it is possible to heat the trapped electrons to a temperature (T_{ep}) that is much higher than that of the passing electrons (T_{ec}). This, in turn, effects a large increase in the potential difference between the plug midplane and the central cell (ϕ_c) without the concomitant increase of plug density, and hence neutral beam injection power, that limited the performance of earlier tandem mirror machines. Indeed, with thermal barriers, a tandem mirror's plug density (n_p) may actually be less than its central cell density (n_c).

Typical potential and density profiles are illustrated in Figure 1, along with the associated vacuum magnetic field profile. Ions are prevented from collisionally accumulating within the barrier region, and thus destroying its potential depression, by means of a pumping scheme consisting of three neutral beams aimed within the barrier cell's loss cone. Charge exchange between a neutral from one of these beams and an ion trapped in the barrier region results in the production of a passing (untrapped) ion and a new neutral which is assumed to leave the plasma. Furthermore, the portions of these beams that ionize rather than charge exchange may be used to at least partially fuel the central cell plasma.

The physics model for this system has been described in detail in the first reference.[1] The model assumes no buildup of thermal alpha particles anywhere in the reactor, that axial (particle and energy) losses of central cell ions and passing electrons are large in comparison with the corresponding radial losses, and that neutrals produced by charge exchange of the pumping beams with ions trapped in the barrier region necessarily leave the plasma. The model includes the calculation of the axial profiles of potential, density, and perpendicular beta throughout the barrier region, given the axial vacuum magnetic field profile used in this region as input. Thus, intrinsic quantitites defined per unit volume of the barrier region (such as synchrotron radiation power, power transfer from trapped to passing electrons, and the current of passing ions that collisionally trap in the barrier) are integrated over these axial profiles to yield the corresponding extrinsic or total quantities. Furthermore, the code is capable of simulating radial density profiles of the form:

$$n_c = n_{c0} \left[1 - \left(\frac{r}{r_c}\right)^{\gamma} \right] \tag{1a}$$

and:

$$n_p = n_{p0} \left[1 - \left(\frac{r}{r_p}\right)^{\gamma} \right] \tag{1b}$$

(where γ is input) in the calculation of total fusion power, wall loading, and radially-averaged perpendicular betas for field reduction. In all other respects, however, the model is zero-dimensional.

Finally, the code is steady-state, solving only for equilibrium configurations, and so questions dealing with start-up, stability, or any other time-dependent behavior are not addressed.

II. SURVEY OF METHOD OF SOLUTION OF PHYSICS MODEL EQUATIONS

This section will assume familiarity with the physics model described in the first reference.[1] The parametric studies code requires as input the following variables:

T_c (central cell ion temperature),

T_{ec} (passing electron temperature),

T_{ep} (trapped electron temperature),

$B_{0c,vac}$ (central cell vacuum field),

$B_{0p,vac}$ (plug midplane vacuum field),

$B_{mp,vac}$ (plug mirror vacuum field),

$B_{0b,vac}$ (barrier midplane vacuum field),

$B_{mb,vac}$ (barrier mirror vacuum field),

β_{c0} (perpendicular beta on axis in central cell),

β_{p0} (perpendicular beta on axis in plugs),

and: ϕ_p (ambipolar potential at plug midplane) = $\phi_e + \phi_c$.

The final two input variables may be either:

r_c (central cell plasma radius),

and: L_c (central cell length);

or: Γ_{FW} (first wall loading of 14 MeV neutrons),

and: P_{FUS} (fusion power).

To solve the equations describing the TMR with thermal barriers, the code proceeds as follows: The central cell perpendicular plasma pressure is given by:

$$P_{\perp c} \simeq n_{c0} (T_c + T_{ec}) + P_{\perp}^{sp\alpha}, \tag{2}$$

where the contribution due to superthermal alphas is modeled by:

$$P_{\perp}^{sp\alpha} \simeq 8.3 \times 10^{10} n_{c0} \langle\sigma v\rangle_{DT} T_{ec}^{3/2} E_{\alpha} f_{\alpha e} . \tag{3}$$

Then since:

$$\beta_{c0} = \frac{P_{\perp c}}{(B_{0c,vac})^2/2\mu_o} , \tag{4}$$

we can solve for the central cell ion density:

$$n_{c0} \simeq \frac{\beta_{c0} (B_{0c,vac})^2}{2\mu_o (T_c + T_{ec} + 8.3 \times 10^{10} \langle\sigma v\rangle_{DT} T_{ec}^{3/2} E_{\alpha} f_{\alpha e})} . \tag{5}$$

In equation (5), $\langle\sigma v\rangle_{DT}$ is a function of T_c alone,[2] and $f_{\alpha e}$ is a function of T_{ec} alone.[3] Thus, all quantities on the right hand side are known from the input, and the code may immediately calculate n_{c0}.

If r_c and L_c are input, the code may next calculate the fusion power:

$$P_{FUS} = \int_0^{r_c} \frac{1}{4} n_c^2 \langle\sigma v\rangle_{DT} E_{FUS} \cdot 2\pi r \, dr \cdot L_c$$

$$\therefore P_{FUS} = \frac{1}{4} n_{c0}^2 \langle\sigma v\rangle_{DT} E_{FUS} \pi r_c^2 L_c \frac{\gamma 2}{(\gamma + 1)(\gamma + 2)} , \tag{6}$$

where we have used equation (1). If we define the "zero-dimensional radius":

$$r_{c0} \equiv r_c \frac{\gamma}{\sqrt{(\gamma + 1)(\gamma + 2)}}, \tag{7}$$

then we may write:

$$P_{FUS} = \frac{1}{4} n_{c0}^2 \langle \sigma v \rangle_{DT} E_{FUS} \pi r_{c0}^2 L_c. \tag{8}$$

The first wall loading of 14 MeV neutrons is given by:

$$\Gamma_{FW} = \frac{(E_n/E_{FUS}) P_{FUS}}{2 \pi r_{FW} L_c}. \tag{9}$$

where r_{FW} is the first wall radius, and is taken to be greater than r_c by three Larmor radii of 3.52 MeV alpha particles in the vacuum magnetic field of the central cell (a function of $B_{0c,vac}$ only). Thus:

$$r_{FW} = r_c + 3\rho_\alpha . \tag{10}$$

If, on the other hand, P_{FUS} and Γ_{FW} are input instead of r_c and L_c, we see that equations (6), (9), and (10) yield:

$$\left[\frac{1}{8} n_{c0}^2 \langle \sigma v \rangle_{DT} E_n \frac{\gamma^2}{(\gamma + 1)(\gamma + 2)}\right] r_c^2 - (\Gamma_{FW}) r_c - (3\rho_\alpha \Gamma_{FW}) = 0 \tag{11}$$

which is a quadratic equation yielding a unique positive solution for r_c. Given this and P_{FUS}, equation (6) may then be solved for L_c.

The profile-averaged perpendicular beta is then calculated in both the central cell and the plug:

$$\bar{\beta}_c = \frac{1}{\pi r_c^2} \int_0^{r_c} \beta_c \cdot 2\pi r \, dr = \left(\frac{\gamma}{\gamma + 2}\right) \beta_{c0}, \tag{12a}$$

and:

$$\bar{\beta}_p = \frac{1}{\pi r_c^2} \int_0^{r_c} \beta_p \cdot 2\pi r \, dr = \left(\frac{\gamma}{\gamma + 2}\right) \beta_{p0}, \tag{12b}$$

where we have used equations (1) and the fact that the betas are proportional to density.

The equation of conservation of magnetic flux is then used to calculate r_p:

$$r_p = r_c \left[\frac{B_{0c,vac}}{B_{0p,vac}} \sqrt{\frac{1 - \bar{\beta}_c}{1 - \bar{\beta}_p}}\right]^{1/2} \tag{13a}$$

and:

$$r_{p0} = r_{c0} \left[\frac{B_{0c,vac}}{B_{0p,vac}} \sqrt{\frac{1 - \bar{\beta}_c}{1 - \bar{\beta}_p}}\right]^{1/2}, \tag{13b}$$

where we have used the "long-thin" approximation in both the central cell and the plugs. From the "zero-dimensional radii", we calculate the "zero dimensional plasma volumes" that are used in the particle and energy balance equations*:

$$V_c = \pi r_{c0}^2 L_c, \tag{14a}$$

and:

$$V_p = \frac{4\pi}{3} r_{p0}^3 . \tag{14b}$$

* Since all terms in these equations that are proportional to a volume are also proportional to a density squared.

Next, the code makes an initial guess of the value of R_b, the plasma mirror ratio in the barrier cell (the vacuum mirror ratio provides a convenient starting guess). Given this guess, the following equation[4] is solved numerically for φ_b:

$$\left(\frac{\phi_b}{T_c}\right) = \left(\frac{T_{ec}}{T_c}\right) \ln\left\{\left(\frac{R_b}{g_{b0}}\right)\left[1 + \pi\left(\frac{\phi_b}{T_c}\right)\right]^{1/2}\right\} \tag{15}$$

Then n_{b0} may be calculated from:[5]

$$n_{b0} = n_{c0} \exp\left(-\frac{\hat{\varphi}_b}{T_{ec}}\right) \tag{16}$$

Given this, the profile-averaged perpendicular beta may be calculated at both the barrier midplane and mirror:

$$\bar{\beta}_{0b} = \frac{n_b\left[(T_c/R_b) + T_{ec}\right]}{\left[(B_{0b,vac})^2/2\mu_o\right]}\left(\frac{\gamma}{\gamma+2}\right), \tag{17a}$$

and:

$$\bar{\beta}_{mb} = \frac{n_c\left[(T_c/R_b) + T_{ec}\right]}{\left[(B_{mb,vac})^2/2\mu_o\right]}\left(\frac{\gamma}{\gamma+2}\right), \tag{17b}$$

where (T_c/R_b) is taken to be the perpendicular ion temperature in the barrier, and $(\gamma/\gamma+2)$ is the profile correction factor in the spirit of equations (12). Finally, we use:

$$R_b = \frac{B_{mb,vac}}{B_{0b,vac}}\sqrt{\frac{1-\bar{\beta}_{mb}}{1-\bar{\beta}_{0b}}} \tag{18}$$

to obtain a better guess for R_b, and the entire process (beginning with equation (15)) is repeated until it converges on a self-consistent set of values for R_b, n_b, ϕ_b, $\bar{\beta}_{0b}$, and $\bar{\beta}_{mb}$.

Since ϕ_p ($\equiv \phi_e + \phi_c$) is input, we have enough information at this point to apply the Logan-Rensink plug model. The details of this model are presented in Reference 6. This model, coupled with the plug beta equation:[7]

$$n_{p0} = \frac{\left(B_{0p,vac}\right)^2 \beta_{p0}}{2\mu_o \left(0.9\ E_p + T_{ep}\right)} , \tag{19}$$

and the plug ion energy balance (neglecting charge exchange):[8]

$$E_p = \frac{\left(E_p^{inj} - \bar{E}_L\right)}{(n\tau)_p} (n\tau)_p^{drag} + \frac{3}{2} T_{ep} , \tag{20}$$

where $\bar{E}_L$ is the average loss energy of plug ions (determined by the plug model), form a set of simultaneous nonlinear equations that may be solved self-consistently for $(n\tau)_p$, n_p, and E_p.

Once n_p is known, we may use:[9]

$$\phi_c = T_{ep} \ln\left(\frac{n_{p0}}{n_{b0}}\right) - \phi_b \tag{21}$$

to find ϕ_c. And ϕ_e is then given by:

$$\phi_e = \phi_p - \phi_c . \tag{22}$$

The potentials at which the pump beams are injected are denoted by ϕ_{LEPB}, ϕ_{MEPB}, and ϕ_{HEPB} for the low, medium and high energy pump beams, respectively. Throughout this study we have used:

$$\phi_{LEPB} = \phi_e + 0.1\,\phi_b, \tag{23a}$$

$$\phi_{MEPB} = \phi_e - 0.5\,\phi_b, \tag{23b}$$

and: $$\phi_{HEPB} = \phi_e - \phi_b, \tag{23c}$$

though, at least in the first two cases, one might wish to experiment with these values.

Given all of the above information, as well as the exact vacuum magnetic field axial profile in the barrier region, it is possible to determine $\phi^*(z)$, $n_0^*(z)$, and $\beta_0^*(z)$; these being the potential, peak density, and peak perpendicular beta profiles throughout the barrier cell, respectively. To accomplish this, the barrier cell is divided up into a large number of subintervals, and three simultaneous nonlinear equations[10] are solved simultaneously to yield ϕ^*, n_0^*, and β_0^* at the midpoint of each subinterval. These equations are presented in Appendix I. Then the subinterval on the barrier's inboard side whose potential ϕ^* is closest to ϕ_{MEPB} is designated as that subinterval at which the medium energy pump beam (MEPB) is injected. The LEPB is similarly "placed" on the barrier's outboard side (the transition region), and the HEPB is "placed" at the barrier midplane.

The plasma cross sectional area as a function of axial position in the barrier region is obtained from the following equation of conservation of magnetic flux:

$$A^*(z) = \pi r_{c0}^2 \left[\frac{B_{0c,vac}}{B^*_{vac}(z)} \sqrt{\frac{1 - \bar{\beta}_c}{1 - \bar{\beta}^*(z)}} \right], \tag{24}$$

where:

$$\bar{\mathcal{E}}^{*}(z) = \left(\frac{\gamma}{\gamma + 2}\right) \mathcal{E}^{*}(z) \ . \tag{25}$$

Then, a differential volume element in the barrier cell is given by:

$$dV^{*} = A^{*}(z)\, dz \tag{26}$$

where dz is the differential element of length in the axial direction.

The current of passing ions that trap in the barrier region per unit barrier volume has been determined from Fokker-Planck calculations and fit to the form:[11]

$$J_{trap}(z) \simeq \left[\frac{n_0^{*}(z)}{g_b(z)}\right]^2 \frac{\left\{1 + 0.35 \left[\frac{B_{mb,vac}\sqrt{1 - \bar{\mathcal{E}}_{mb}}}{B_{vac}^{*}(z)\sqrt{1 - \bar{\mathcal{E}}^{*}(z)}}\right]\right\}}{5.5 \times 10^{9}\, T_c^{3/2}} \tag{27}$$

The total charge exchange pumping current required is then obtained by integrating over the length of the barrier region:

$$I_{trap} = 2e \int_{z_{mb}}^{z_{mp}} J_{trap}(z)\, dV^{*} \tag{28}$$

where the factor of 2 accounts for both ends of the machine.

The power transfer from trapped to passing electrons in both transition regions is:[12]

$$P_{cp}^{*} \simeq 2 \int_{z_{0b}}^{z_{mp}} G_{et} \frac{n_{p0}^{2}}{(n\tau)_t^{ee}} (T_{ep} - T_{ec}) \exp\left[-\frac{\phi_e + \phi_c - \phi^{*}(z)}{T_{ep}}\right] dV^{*}, \tag{29}$$

and that in the plug is:[13]

$$P_{cp} \simeq 2G_{ep} \frac{n_{p0}^2}{(n\tau)_p^{ee}} (T_{ep} - T_{ec}) \exp\left(-\frac{\dot{\varphi}_c + \dot{\varphi}_b}{T_{ep}}\right) V_p \ ; \tag{30}$$

where:

$$G_{ep} \simeq G_{et} \simeq 1, \tag{31}$$

$$(n\tau)_p^{ee} \simeq 8.19 \times 10^9 \frac{T_{ep}^{3/2}}{\ln \Lambda_p^{ee}} \ , \tag{32}$$

$$(n\tau)_t^{ee} \simeq 8.19 \times 10^9 \frac{T_{ep}^{3/2}}{\ln \Lambda_t^{ee}} \ , \tag{33}$$

$$\ln \Lambda_p^{ee} \simeq \ln\left[(2.83 \times 10^{13}) \, T_{ep} / \sqrt{n_{p0}}\right] , \tag{34}$$

$$\ln \Lambda_t^{ee} \simeq \ln\left[(2.83 \times 10^{13}) \, T_{ep} / \sqrt{n^*(z)}\right] , \tag{35}$$

The synchrotron radiation power lost in the transition regions is given by the non-relativistic expression:

$$P_{sync}^* \simeq 2 \int_{z_{0b}}^{z_{mp}} (0.3745) \left[B_{vac}^*(z)\right]^2 \cdot \left[1 - \bar{\beta}^*(z)\right] \left[n_0^*(z) - n_{b0}\right] T_{ep} \sqrt{1-R} \ dV^* \ , \tag{36}$$

and that in the plugs is:

$$P_{sync} \simeq 2 \cdot (0.3745) \left[B_{0p,vac} \sqrt{1 - \bar{\beta}_p}\right]^2 n_{p0} \, T_{ep} \sqrt{1-R} \ V_p , \tag{37}$$

where R is the reflectivity of the surrounding wall, taken equal to zero in order to be pessimistic in these studies.

The final step in solving the physics model equations is that of satisfying the particle and energy balance equations. These equations are listed in Appendix II. In these equations, we have used the following variables:

f_D ≡ (fraction of trapped barrier ions removed passively by drifts[14])

f_{LEPB} ≡ (fraction of trapped barrier ions not removed passively that are removed by the low energy pump beam)

f_{MEPB} ≡ (fraction of trapped barrier ions not removed passively that are removed by the medium energy pump beam)

f_{HEPB} ≡ (fraction of trapped barrier ions not removed passively that are removed by the high energy pump beam)

I_{AUX} ≡ (auxiliary fueling current of D-T ions entering central cell at an energy $E_{c,inj}$)

To solve these equations, we note that the passing electron particle balance, passing electron energy balance, central cell ion particle balance, and central cell ion energy balance are all linear in the five variables:

$$X_1 = f_D, \tag{38a}$$

$$X_2 = (1 - f_D)\, f_{LEPB}, \tag{38b}$$

$$X_3 = (1 - f_D)\, f_{MEPB}, \tag{38c}$$

$$X_4 = (1 - f_D)\, f_{HEPB}, \tag{38d}$$

$$X_5 = I_{AUX}\ . \tag{38e}$$

The fifth equation required to determine the system is the condition that the fractions of trapped particles pumped by each of the three energetic pump beams add to one:

$$f_{LEPB} + f_{MEPB} + f_{HEPB} = 1.$$

This may be written:

$$f_D + (1 - f_D)\, f_{LEPB} + (1 - f_D)\, f_{MEPB} + (1 - f_D)\, f_{HEPB} = 1. \qquad (39)$$

Thus we have five linear equations in five unknowns, and so the system is easily solved for X_1, through X_5. Then:

$$f_D = X_1, \qquad (40a)$$

$$f_{LEPB} = X_2/(1 - X_1)\ , \qquad (40b)$$

$$f_{MEPB} = X_3/(1 - X_1)\ , \qquad (40c)$$

$$f_{HEPB} = X_4/(1 - X_1)\ , \qquad (40d)$$

and: $$f_{AUX} = X_5\ . \qquad (40e)$$

The only remaining balance equation, namely the trapped electron energy balance, is then solved for the required ECRH input power, P_{ECRH}. This amounts to no more than solving a linear equation, and completes the determination of the system. The plasma Q is then given by:

$$Q = \frac{P_{FUS}}{P_{PUMP} + P_{NB}^{plug} + P_{NB}^{cc} + P_{ECRH}} \qquad (41)$$

where P_{PUMP} is the pumping power, P_{NB}^{plug} is the plug neutral beam power, P_{NB}^{cc} is the central cell neutral beam power if any (equal to zero in these studies since $E_{c,inj}$ is taken to be zero).

III. OPTIMIZATION TECHNIQUES

The solution technique outlined in section II is relatively easy to apply, but is unusual in the respect that one must input T_c, T_{ec}, T_{ep} and ϕ_p, while f_D, f_{LEPB}, f_{MEPB}, and f_{HEPB} are output quantities. These output quantities are subject to the constraints:

$$0 \leq f_{LEPB} \leq 1, \tag{42a}$$

$$0 \leq f_{MEPB} \leq 1, \tag{42b}$$

$$0 \leq f_{HEPB} \leq 1, \tag{42c}$$

and:
$$0 \leq f_D \leq 1/2. \tag{42d}$$

The first three of these conditions are obvious, given the definition of f_{LEPB}, f_{MEPB}, and f_{HEPB}. The fourth condition is due to the fact that 1/2 is currently believed to be the upper bound for the fraction of trapped barrier ions that may be passively removed by virtue of their extended drift surfaces.

Define the vectors:

$$\underline{y} \equiv \begin{pmatrix} f_{LEPB} \\ f_{MEPB} \\ f_{HEPB} \\ f_D \\ Q \end{pmatrix} \tag{43a}$$

and

$$\underline{x} \equiv \begin{pmatrix} T_c \\ T_{ec} \\ T_{ep} \\ \phi_p \\ B_{0c,vac} \end{pmatrix}. \tag{43b}$$

Then, the solution technique outlined in section II may be thought of as a vector function $\underline{F}$ mapping $\mathbb{R}^5 \rightarrow \mathbb{R}^5$:

$$\underline{y} = \underline{F}(\underline{x}). \tag{44}$$

Equations (42) constrain the range of the functon $\underline{F}$, and this in turn constrains its domain. We refer to a simply-connected subset of the domain of $\underline{F}$, such that the range of $\underline{F}$ satisfies equations (42), as an "island" of solution. In general, there may be several disjoint islands of solution in the domain of $\underline{F}$. The union of these islands constitutes the totality of physical solutions to the problem.

In all of the studies conducted thusfar, the fusion power and wall loading have been fixed, and the desire has been to maximize Q. In light of the above considerations, this problem becomes twofold: (1) To search the domain of interest to find the island(s) of solution; and (2) to search the island(s), once it (they) are found, to find the maximum value of Q physically attainable.

To accomplish both of these ends, we define our figure of merit in the following way:

$$\mathcal{F}(\underline{x}) \equiv \begin{cases} Q & \text{if the conditions of equations (42) are satisfied} \\ -\left(f_{LEPB} - \frac{1}{3}\right)^2 - \left(f_{MEPB} - \frac{1}{3}\right)^2 - \left(f_{HEPB} - \frac{1}{3}\right)^2 - \left(f_{D} - \frac{1}{4}\right)^2 & \text{otherwise} \end{cases} \tag{45}$$

Thus, if we are not on the island, our figure of merit is a four-dimensional paraboloid whose apex is on the island. In this way, by using a simple ascent algorithm, it is possible to both find the island(s) of solution and explore it (them) for a local maximum.

It is evident from equation (45) that the figure of merit is discontinuous at an island's periphery, so our ascent algorithm must be able to cope with this. What is more, the global maximum of $\mathcal{F}$ usually occurs at an island's periphery where the gradient $\partial Q/\partial \underline{x}$ is not necessarily zero, and where

$\partial\tilde{\mathcal{H}}/\partial\underline{x}$ is not even defined. The "island" of solution may be thought of as being surrounded by "cliffs" that drop into the "ocean" of parameter space in which equations (42) are not satisfied. The global maximum of $\tilde{\mathcal{H}}$ usually occurs right on the brink of one of these "cliffs".

The ascent algorithm chosen for these studies is a version of Rosenbrock's method that does not use derivatives in its line searches (i.e. the version originally proposed by Rosenbrock). A detailed description of the algorithm may be found in Reference 15.

Throughout the parametric studies described in the next section, many instances were found in which there seemed to be more than one island of solution, and in which each island had several (up to ten) local maxima (or, at least, points which caused the Rosenbrock algorithm to stall). Since we are interested only in the global maximum, a Monte Carlo scheme was used to generate starting points for the Rosenbrock algorithm within a large region of interest in parameter space. It should always be kept in mind, however, that one can never really be sure that one has found the global maximum. This is because the hypervolume of parameter space from which the ascent algorithm converges on the global maximum may be very small in comparison to the total hypervolume of parameter space that is searched. Thus the results in the following section ought to be thought of as the "greatest lower bound yet discovered" on the global maximum.

IV. RESULTS

A point design is presented in Table 1b. This reactor produces 3500 MW of fusion power at a neutron first wall loading of 1.3 MW/m^2. Its central cell plasma is 217 meters long and 1.29 meters in radius. A cubic density

Table 1. Optimized Point Designs at peak Central Cell beta values of 0.2, 0.4, and 0.7, respectively.

	Table 1a	Table 1b	Table 1c
$n_{c0}(cm^{-3})$	1.421×10^{14}	1.528×10^{14}	1.310×10^{14}
T_c(keV)	25.18	19.30	21.38
T_{ec}(keV)	28.74	22.99	24.10
$B_{0c,vac}$(T)	4.441	2.795	2.050
β_{c0}	0.20	0.40	0.70
I_{aux}(A)	1495.	2147.	2036.
ϕ_c (keV)	202.3	169.4	173.3
r_c (cm)	103.5	128.9	156.3
L_c (m)	281.2	216.9	174.9
n_{p0} (cm^{-3})	2.112×10^{13}	2.182×10^{13}	2.211×10^{13}
E_p (keV)	1000.	1000.	1000.
T_{ep} (keV)	206.1	171.0	156.8
$B_{0p,vac}$ (T)	3.960	3.960	3.960
$B_{mp,vac}$ (T)	5.920	5.920	5.920
β_{p0}	0.60	0.60	0.60
E_p^{inj} (keV)	400.0	400.0	400.0
r_p (cm)	118.7	113.0	109.7
n_{b0} (cm^{-3})	8.013×10^{12}	8.448×10^{12}	7.473×10^{12}
g_{b0}	2.00	2.00	2.00
$B_{0b,vac}$ (T)	1.16	1.16	1.16
$B_{mb,vac}$ (T)	12.0	12.0	12.0
β_{0b0}	0.0746	0.0628	0.0584
β_{mb0}	0.0124	0.0106	0.0096
I_{trap} (A)	3514.	5112.	3422.
f_D	0.4484	0.3721	0.4931
f_{LEPB}	0.8045	0.9769	0.8605
f_{MEPB}	0.1082	0.0017	0.1131
f_{HEPB}	0.0874	0.0214	0.0265
L_b (m)	9.0	9.0	9.0
P_{PUMP} (MW)	84.49	24.38	38.90
P_{NB}^{plug} (MW)	13.10	4.174	4.569
P_{ECRH} (MW)	212.0	216.5	149.8
Γ_{FW} (MW/m^2)	1.30	1.30	1.30
P_{FUS} (MW)	3500.	3500.	3500.
Q	11.31	14.38	18.11

profile ($\gamma = 3$) was assumed and β_{c0} was taken to be 0.4. The maximum value of Q found was 14.28 (only global maxima with respect to each of the components of $\underline{x}$ in equation (43) are reported).

The vacuum magnetic field, potential, and density profiles in the barrier region of the point design (see Table 1b) are plotted in Figure 2. A rather disturbing feature of these profiles is the discontinuous behavior at $z = z_{mb}$ and just to the right of $z = z_{0b}$. These discontinuities occur in the potential and density profiles in spite of the fact that these profiles are the solutions of equations that vary continuously with z (see Appendix I). Though they are undoubtedly not physical, they are probably approximations to physical profiles that are, though continuous, very steep. Thus, any attempt to artifically remove these discontinuities was thought to be a detraction from the model's accuracy--as well as being ad hoc.

During the optimization studies, it was found that the figure of merit often optimized at a point at which $f_{HEPB} = 0$. Evidently, this happened in order to decrease the pumping power as much as possible. Some high energy pump beam is always necessary, however, because the HEPB is the only means available to pump well-trapped ions at the bottom of the barrier's potential depression. The minimum value estimated[16] for f_{HEPB} is 0.02, so we replace equation (42c) with the condition:

$$0.02 \leq f_{HEPB} \leq 1. \tag{46}$$

An interesting tradeoff was observed between the low and medium energy pump beam fractions. Increasing f_{LEPB} and decreasing f_{MEPB} decreases the pumping power for obvious reasons, but, since the low energy pump beam is injected into the transition region, it introduces cold electrons that have to

be heated to a temperature T_{ep}. The effect is thus to trade off pumping power for ECRH power, and the global optimum has been observed to occur at either one extreme or the other, or somewhere in the middle, depending on the specific details of the case being considered.

The point design assumes a peak central cell beta of 0.4. The maximum achievable value of peak central cell beta is fixed by the requirement of stability with respect to the MHD ballooning mode. As this requirement is a subject of ongoing study, it is interesting to examine how the above case scales with β_{c0}. Thus, Tables 1a and 1c present optimized cases at β_{c0} = 0.2 and β_{c0} = 0.7, respectively.

References

1. G. A. Carlson, B. Arfin, W. L. Barr, B. M. Boghosian, J. L. Erickson, J. H. Fink, G. W. Hamilton, B. G. Logan, J. O. Myall, and W. S. Neef, Jr., Tandem Mirror Reactor with Thermal Barriers, Lawrence Livermore Laboratory Report UCRL-52836, (September 1979).
2. ibid, p. 38, equation (2-22).
3. ibid, p. 38, equation (2-21)
4. ibid, p. 41, equation (2-31)
5. ibid, p. 39, equation (2-24)
6. ibid, pp. 48-51
7. ibid, p. 51, equation (2-69)
8. ibid, p. 50, equation (2-65)
9. ibid, p. 39, equation (2-26)
10. ibid, p. 42, equations (2-33), (2-34), (2-35)
11. ibid, p. 43, equation (2-41)
12. ibid, p. 55, equations (2-86), (2-87), (2-88), (2-89b)
13. ibid, pp. 55-56, equation (2-85), (2-87), (2-88), (2-89a)
14. J. Kesner, Passive Generation of Ambipolar Potential Barriers in a Tandem Mirror, University of Wisconsin Report UWFDM-303 (May, 1979).
15. M. S. Bazaraa, C. M. Shetty, Nonlinear Programming, Theory and Algorithms, John Wiley and Sons, Inc., (1979).
16. op cit, G. A. Carlson, et al., pp. 131-132.

Appendix I

EQUATIONS FOR DENSITY POTENTIAL AND PERPENDICULAR BETA AXIAL PROFILES IN BARRIER REGION

The profile of g_b, the ratio of total ion density to passing ion density in the barrier cell, is given by:

$$g_b(z) = 1 + (g_{b0} - 1) \frac{\left[1 - \frac{B^*_{vac}(z)}{B_{bm,vac}}\right]}{\left[1 - \frac{B_{b0,vac}}{B_{bm,vac}}\right]} \tag{I-1}$$

Given this, the peak density n_0^*, plasma potential *, and peak perpendicular beta $^*_0$ may be calculated at any position z in the barrier cell by solving the following three equations simultaneously:

$$n_0^*(z) = g_b(z)\, n_{c0} \frac{B^*_{vac}(z)}{B_{mb,pla}} [1 - \beta_0^*(z)]^{1/2} \left\{\frac{T_c}{\pi[\phi_e - \phi^*(z)] + T_c}\right\}^{1/2} \quad \text{for } \phi^* \leq \phi_e \ , \tag{I-2a}$$

$$n_0^*(z) = g_b(z) n_{c0} \frac{B^*_{vac}(z)}{B_{mb,pla}} [1 - \beta_0^*(z)]^{1/2} \left[\frac{\exp\left(-\frac{\phi^*(z) - \phi_e}{T_c}\right) - \exp\left(-\frac{\phi_c}{T_c}\right)}{1 - \exp\left(-\frac{\phi_c}{T_c}\right)}\right] \tag{I-2b}$$

$$\text{for } \phi^* > \phi_e \ ,$$

$$\phi^*(z) = \phi_e - T_{ec} \ln [n_{c0}/n_0^*(z)] \quad \text{for } z \leq z_{b0} \ , \tag{I-3a}$$

$$\phi^*(z) = \phi_e + \phi_c - T_{ep} \ln [n_{p_0}/n_0^*(z)] \quad \text{for } z \geq z_{b0} \quad , \tag{I-3b}$$

$$\beta_0^*(z) = [n_0^*(z)\ (T_c/R_b) + n_0^*(z)\ T_{ec}] \Big/ \left\{[B_{vac}^*(z)]^2 \Big/ 2\mu_0\right\} \quad \text{for } z \leq z_{b0}, \tag{I-4a}$$

$$\beta_0^*(z) = \left\{n_0^*(z)\ (T_c/R_b) + [n_0^*(z) - n_{b_0}]\ T_{ep} + n_{b_0} T_{ec}\right\} \Big/ \left\{[B_{vac}^*(z)]^2 \Big/ 2\mu_0\right\} \quad \text{for } z \geq z_{b0} \tag{I-4b}$$

Detailed descriptions of these equations may be found in Chapter 2 of Reference 1.

Appendix II

PARTICLE AND ENERGY BALANCE EQUATIONS

The total pump beam currents are given by:

$$I_{LEPB} = (1 - f_D)\, f_{LEPB} \left[\frac{g_b(z_{LEPB})}{g_b(z_{LEPB}) - 1}\right] \left(1 + \frac{\langle\sigma v\rangle^{ion}_{LEPB}}{\langle\sigma v\rangle^{cx}_{LEPB}}\right) I_{TRAP} \quad , \tag{II-1a}$$

$$I_{MEPB} = (1 - f_D)\, f_{MEPB} \left[\frac{g_b(z_{MEPB})}{g_b(z_{MEPB}) - 1}\right] \left(1 + \frac{\langle\sigma v\rangle^{ion}_{MEPB}}{\langle\sigma v\rangle^{cx}_{MEPB}}\right) I_{TRAP} \quad , \tag{II-1b}$$

and

$$I_{HEPB} = (1 - f_D)\, f_{HEPB} \left[\frac{g_b(z_{HEPB})}{g_b(z_{HEPB}) - 1}\right] \left(1 + \frac{\langle\sigma v\rangle^{ion}_{HEPB}}{\langle\sigma v\rangle^{cx}_{HEPB}}\right) I_{TRAP} \quad . \tag{II-1c}$$

The superscripts "ion" and "cx" shall be used to denote the ionization and charge exchange fractions of these currents, respectively. The gas pump current is then:

$$I_{GP} = f_D\, I_{TRAP} \tag{II-2}$$

The central cell ion particle balance equation is written:

$$\frac{n_{c0}^2 V_c}{(n\tau)_c} + \frac{1}{2} n_{c0}^2 \langle\sigma v\rangle_{DT} V_c + I_{GP} = I_{LEPB}^{ion} + I_{MEPB}^{ion} + I_{HEPB}^{ion} + I_{AUX}^{ion} \quad , \tag{II-3}$$

where

$$I_{AUX}^{ion} \equiv \frac{\langle\sigma v\rangle_{AUX}^{ion}}{\langle\sigma v\rangle_{AUX}^{ion} + \langle\sigma v\rangle_{AUX}^{cx}} I_{AUX} \tag{II-4a}$$

and

$$I_{AUX}^{cx} \equiv \frac{\langle\sigma v\rangle_{AUX}^{cx}}{\langle\sigma v\rangle_{AUX}^{ion} + \langle\sigma v\rangle_{AUX}^{cx}} I_{AUX} \tag{II-4b}$$

comprise an auxiliary fuel source located at the central-cell potential,

$$(n\tau)_c \approx 5.547 \times 10^{11} \frac{g(R_{ci}/2)}{\ln \Lambda_{ii}} T_c^{3/2} \left(\frac{\phi_c}{T_c}\right) \exp\left(\frac{\phi_c}{T_c}\right) \tag{II-5}$$

is the Pastukhov $(n\tau)$,

$$R_{ci} \equiv B_{Op,pla}/B_{cc,pla} \quad , \tag{II-6}$$

$$\ln \Lambda_{ii} = \ln \left[3.08 \times 10^{14} \left(\frac{T_c^{3/2}}{n_{c0}^{1/2}}\right)\right] , \tag{II-7}$$

and

$$g(x) \equiv \frac{\sqrt{\pi}}{2} \left(1 + \frac{1}{x}\right)^{1/2} \ln\left\{\left[\left(1 + \frac{1}{x}\right)^{1/2} + 1\right] \Big/ \left[\left(1 + \frac{1}{x}\right)^{1/2} - 1\right]\right\} . \tag{II-8}$$

The central cell ion energy balance equation is written:

$$\frac{1}{4} n_{c0}^2 \langle\sigma v\rangle_{DT} \left[E_\alpha \left(1 + \frac{E_R}{E_{FUS}}\right) f_{\alpha i} - E_R\right] V_c - \frac{n_{c0}^2 V_c}{(n\tau)_c} (\phi_c + T_c)$$

$$+ \frac{n_{c0}^2 V_c}{(n\tau)_{ei}} \cdot \frac{3}{2} (T_{ec} - T_c) + \left[I_{AUX}^{ion} E_{c,inj} + I_{AUX}^{cx} (E_{c,inj} - \frac{3}{2} T_c)\right.$$

$$+ I_{LEPB}^{ion} (V_{LEPB} + \phi_{LEPB} - \phi_e) + I_{LEPB}^{cx} (V_{LEPB} + \phi_{LEPB} - \phi_e - \frac{3}{2} T_c)$$

$$+ I_{MEPB}^{ion} (V_{MEPB} + \phi_{MEPB} - \phi_e) + I_{MEPB}^{cx} (V_{MEPB} + \phi_{MEPB} - \phi_e - \frac{3}{2} T_c)$$

$$+ I_{HEPB}^{ion} (V_{HEPB} + \phi_{HEPB} - \phi_e) + I_{HEPB}^{cx} (V_{HEPB} + \phi_{HEPB} - \phi_e - \frac{3}{2} T_c)$$

$$\left. - I_{GP} (\frac{3}{2} T_c)\right] \Big/ e = 0, \qquad \text{(II-9)}$$

where

$$E_R \approx 45.0 + \frac{3}{2} T_c \quad , \qquad \text{(II-10)}$$

$$(n\tau)_{ei} \approx \frac{2.50 \times 10^{13} T_{ec}^{3/2}}{\ln \Lambda_{ei}} \qquad \text{(II-11)}$$

and

$$\ln \Lambda_{ei} \approx \ln [2.65 \times 10^{13} T_{ec}/\sqrt{n_{c0}}] \quad . \qquad \text{(II-12)}$$

The passing electron particle balance is then:

$$(I^{ion}_{LEPB} + I^{ion}_{MEPB} + I^{ion}_{HEPB} + I^{ion}_{AUX} + I_s)/e + \frac{n^2_{p0}(2V_p)}{(n\tau)_p} = \frac{n^2_{c0}V_c}{(n\tau)_{ec}} \quad , \tag{II-13}$$

where

$$(n\tau)_{ec} \approx 4.10 \times 10^9 \frac{g(R_{ce})}{\ln \Lambda_{ee}} T^{3/2}_{ec} \left(\frac{\phi_e}{T_{ec}}\right) \exp\left(\frac{\phi_e}{T_{ec}}\right) \quad , \tag{II-14}$$

and

$$\ln \Lambda_{ee} \approx \ln (2.83 \times 10^{13} T_{ec}/\sqrt{n_{c0}}) \quad . \tag{II-15}$$

The passing electron energy balance may be written:

$$\begin{aligned} &\frac{1}{4} n^2_{c0} \langle\sigma v\rangle_{DT} \left[E_\alpha \left(1 + \frac{E_R}{E_{FUS}}\right) f_{\alpha e}\right] V_c + \frac{1}{e} I_s \phi_e \\ &- \frac{n^2_{c0}V_c}{(n\tau)_{ec}} (\phi_e + T_{ec}) + \frac{n^2_{p0}(2V_p)}{(n\tau)_p} (\phi_b + T_{ep}) - \frac{n^2_{c0}V_c}{(n\tau)_{ei}} \cdot \frac{3}{2} (T_{ec} - T_c) \\ &+ P^*_{cp} + P_{cp} = \frac{-1}{e} \left[I^{ion}_{LEPB} (\phi_b + \overline{E}_{e\ LEPB}) \right. \\ &\qquad + I^{ion}_{MEPB} (\phi_e - \phi_{MEPB}) \\ &\qquad \left. + I^{ion}_{HEPB} (\phi_b)\right] \quad , \end{aligned} \tag{II-16}$$

where

$$\overline{E}_{e\ LEPB} \approx \phi_b + \phi_{LEPB} - \phi_e \quad , \tag{II-17}$$

Finally, the trapped electron energy balance is given by:

$$P_{ECRH} + \frac{n_{p0}^2 (2V_p)}{(n\tau)_{drag}} \left(E_p - \frac{3}{2} T_{ep}\right) - \frac{n_{p0}^2 (2V_p)}{(n\tau)_p} \left(\phi_c + \phi_b + T_{ep}\right)$$

$$= P_{cp}^* + P_{cp} + P_{synchrotron} + \frac{1}{e} I_{LEPB}^{ion} \left[\left(\phi_{LEPB} + \phi_b - \phi_e\right) + \bar{E}_{e\ LEPB}\right]. \quad \text{(II-18)}$$

Descriptions of each term of each of these equations may be obtained in Chapter 2 of Reference 1.

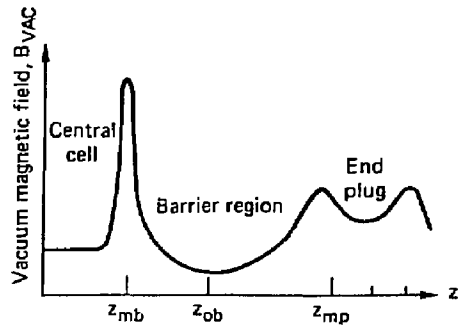

Fig. 1a. Vacuum magnetic field profile.

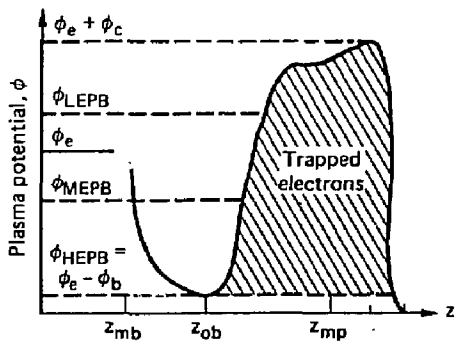

Fig. 1b. Plasma potential profile.

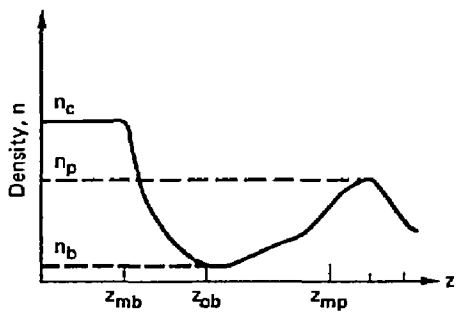

Fig. 1c. Ion density profile.

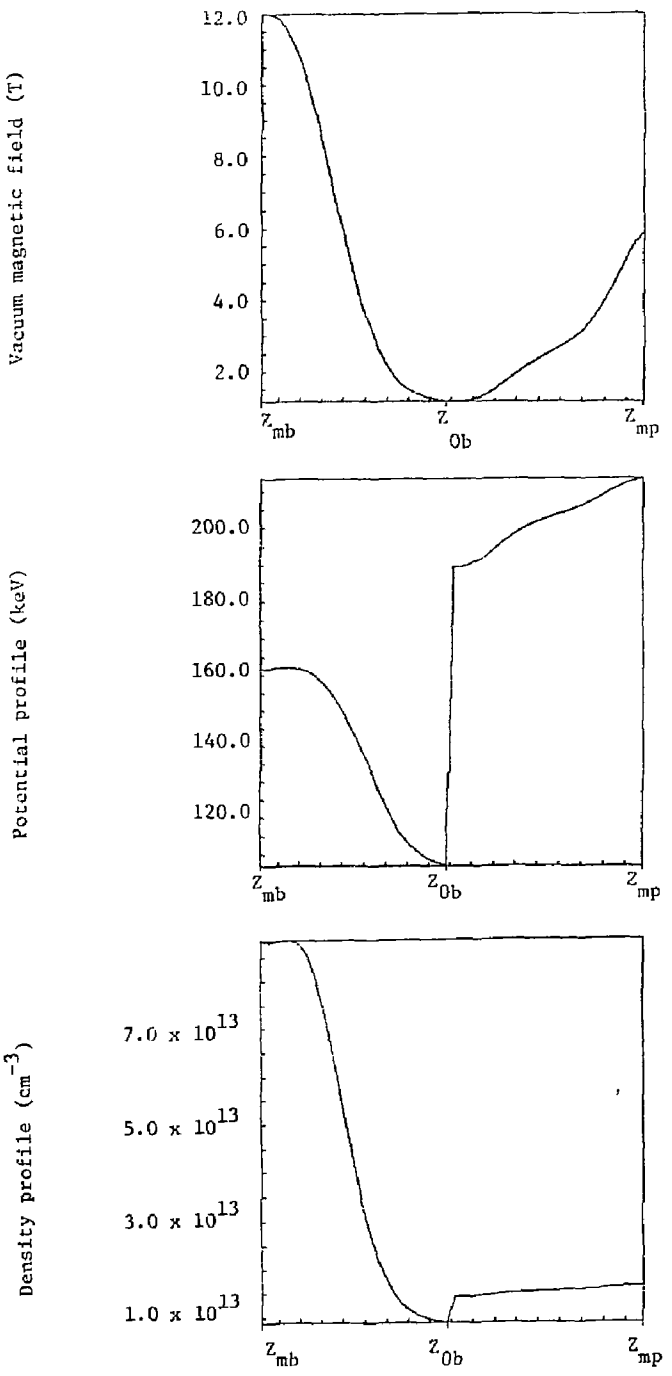
Vacuum magnetic field (T)
12.0
10.0
8.0
6.0
4.0
2.0
Z_{mb}
Z_{0b}
Z_{mp}
Potential profile (keV)
200.0
180.0
160.0
140.0
120.0
Z_{mb}
Z_{0b}
Z_{mp}
Density profile (cm^{-3})
7.0×10^{13}
5.0×10^{13}
3.0×10^{13}
1.0×10^{13}
Z_{mb}
Z_{0b}
Z_{mp}

Figure 2.